Materials and Manufacturing Processes
Publication details, including instructions for authors and subscription information:
http://www.tandfonline.com/loi/lmmp20

Prediction of Mechanical Properties in Submerged Arc Weld Metal of C-Mn Steel

Prasanta Kanjilal [a], Tapan Kumar Pal [b] & Sujit Kumar Majumdar [c]

[a] Mechanical Engineering Division, National Test House, Salt Lake, Kolkata, India

[b] Metallurgical Engineering Department, Jadavpur University, Kolkata, India

[c] SQC and OR Division, Indian Statistical Institute, Kolkata, India

Available online: 02 Mar 2007

To cite this article: Prasanta Kanjilal, Tapan Kumar Pal & Sujit Kumar Majumdar (2007): Prediction of Mechanical Properties in Submerged Arc Weld Metal of C-Mn Steel, Materials and Manufacturing Processes, 22:1, 114-127

To link to this article: http://dx.doi.org/10.1080/10426910601016038

Prediction of Mechanical Properties in Submerged Arc Weld Metal of C–Mn Steel

PRASANTA KANJILAL[1], TAPAN KUMAR PAL[2], AND SUJIT KUMAR MAJUMDAR[3]

[1]*Mechanical Engineering Division, National Test House, Salt Lake, Kolkata, India*
[2]*Metallurgical Engineering Department, Jadavpur University, Kolkata, India*
[3]*SQC and OR Division, Indian Statistical Institute, Kolkata, India*

The prediction model has been developed for steel weld metal mechanical properties as a function of flux ingredients such as CaO, MgO, CaF_2 and Al_2O_3 in submerged arc welding carried out at fixed welding parameters. The results of quantitative measurements of mechanical properties on eighteen weld metal samples were utilized for developing the prediction equations of mechanical properties applying statistical design of experiment for mixtures. Among the flux ingredients, MgO appears to be important on its own in influencing the mechanical properties. The other ingredient CaO appears to be most important as it interacts with CaF_2 and Al_2O_3 in influencing weld metal mechanical properties. The prediction equations have been checked for adequacy by performing tests on submerged arc welds using randomly designed flux and found satisfactory. The ISO-response curves were developed for weld metal impact toughness to show the output levels at different percentage of flux ingredients.

Keywords Acicular ferrite; Binary antagonism; Binary synergism; Carbon equivalent; Extreme vertices design; Flux ingredients; Oxygen content; Prediction model; Statistical experiments.

INTRODUCTION

Submerged arc welding (SAW) is preferred over other arc-welding processes such as MMAW, GTAW, and GMAW due to its high deposition rates, excellent surface finish and ease of automation [1]. However, inherent advantages of the SAW process can be limited by high dilution and low cooling rate which have a tendency to promote low toughness microstructure in the weld metal [2, 3]. Nevertheless, it appears that satisfactory mechanical properties can be obtained through proper selection of flux composition for a given base plate and filler wire. Therefore, there is a need for efficient flux selection in order to provide consistent weld quality because quality assurance schemes for critical applications are becoming increasingly stringent.

Several phenomena associated with the flux behavior during SAW have made if more complicated to control the weld metal composition which ultimately controls the mechanical properties of weld metal. Therefore, many studies [4–9] have tried to understand the behavior of flux in order to control weld metal chemistry. The effects of individual flux ingredients as well as their interaction effects on weld metal composition have been investigated by the authors [10, 11].

Along with the composition, weld metal mechanical properties are also influenced by its microstructure. Several microstructural constituents that can be obtained in weld metal of C–Mn steel are grain boundary ferrite (GBF), side plate ferrite (SPF), polygonal ferrite (PF), and ferrite with aligned second phase (FAS, also known as upper bainite) [12, 13]. It has been recognized that increasing the amount of acicular ferrite (AF) provides both increased toughness and improved strength of the weld joint [14, 15]. Factors such as alloy hardenability, oxygen content, inclusion characteristics and cooling rate play a very important role in determining different microstructure constituents in weld metal [16–18]. Oxygen has a fundamental role in SAW chemistry and transformation behavior, which in turn controls microstructure of the weld metal [19, 20]. The effects of individual flux ingredients as well as their binary interactions on the formation of microstructural constituents in weld metal of C–Mn steel have also been investigated by the authors [21].

In the present studies on submerged arc welding, experimental models have been developed to predict and quantify the effect of each flux ingredient (CaO, MgO, CaF_2, and Al_2O_3) and their binary interactions on weld metal mechanical properties with the application of statistical design of mixture experiments, in particular, extreme vertices design. The aim is to develop satisfactory regression models as shown schematically in Fig. 1, involving proportions of flux ingredients and weld metal mechanical properties, so that the fluxes can be effectively used to achieve target values of the weld metal mechanical properties in the interacting and constrained submerged arc welding atmosphere. The direct relations between the flux ingredients and mechanical properties will be a useful tool for the flux designer for better SAW flux consumables to reach the desired values of weld metal mechanical properties.

PLANNING OF THE EXPERIMENTS

Extreme Vertices Design Algorithm

In experiments using a mixture of q components, the components are expressed as a fraction x of the total

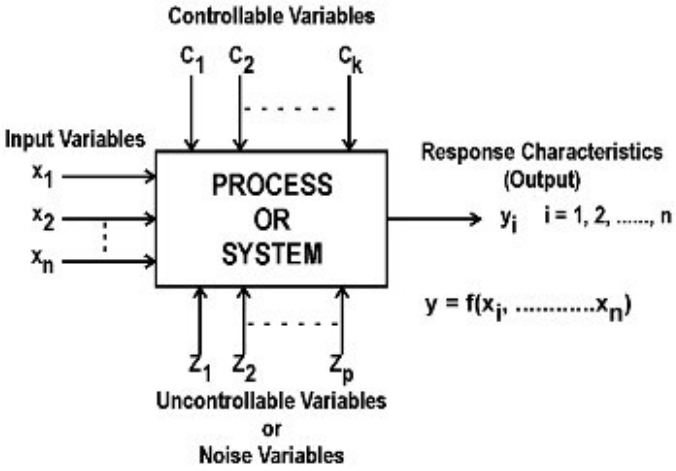

FIGURE 1.—General model of a process or system in statistical mixture design experiment.

mixture, and the response is a function of the proportions of the components and not the total amount of mixture. The extreme vertices design that was used for experimentation [22–24] consisted of the ten admissible vertices of the polyhedron, seven centroids of the seven two-dimensional faces and the overall centroid. Thus although ten coefficients of the quadratic regression model (as shown in Eq. (1)) for the response characteristics were required to be estimated, 18 design points were deliberately chosen for getting better estimates of the coefficients and error. The above design was obtained by following the two step procedures of Mclean and Anderson [23]. After having generated $4 \times 2^{4-1} = 32$ possible combinations of the four components, it was found that there were ten admissible vertices which satisfied the constraint for the mixture total as the lower and upper bounds of each component proportion. The seven two-dimensional faces of the polyhedron were found by grouping the vertices of the polyhedron into groups of three or more vertices where each vertex had the same value x_i for one of the four components. Thus, the coordinates of the seven two-dimensional faces which satisfied the constraints are the design points sl. 11 to 17. The design point sl. no. 18 was the overall centroid which was the average of all ten vertices. The trace $(x'x)^{-1}$, where x represents the complete design matrix of the given design was also small. In 3-D space the constraint design regent is shown in Fig. 2(a) which represents the mixture space in the present experiment.

$$y = \sum_{i=1}^{q} \beta_i x_i + \sum_{i<j}^{q} \sum \sigma_q \beta_{ij} x_i x_j \tag{1}$$

Snee [25] also gave the algorithm for selecting the subsets of extreme vertices for fitting quadratic models of the following form in the constrained mixture spaces.

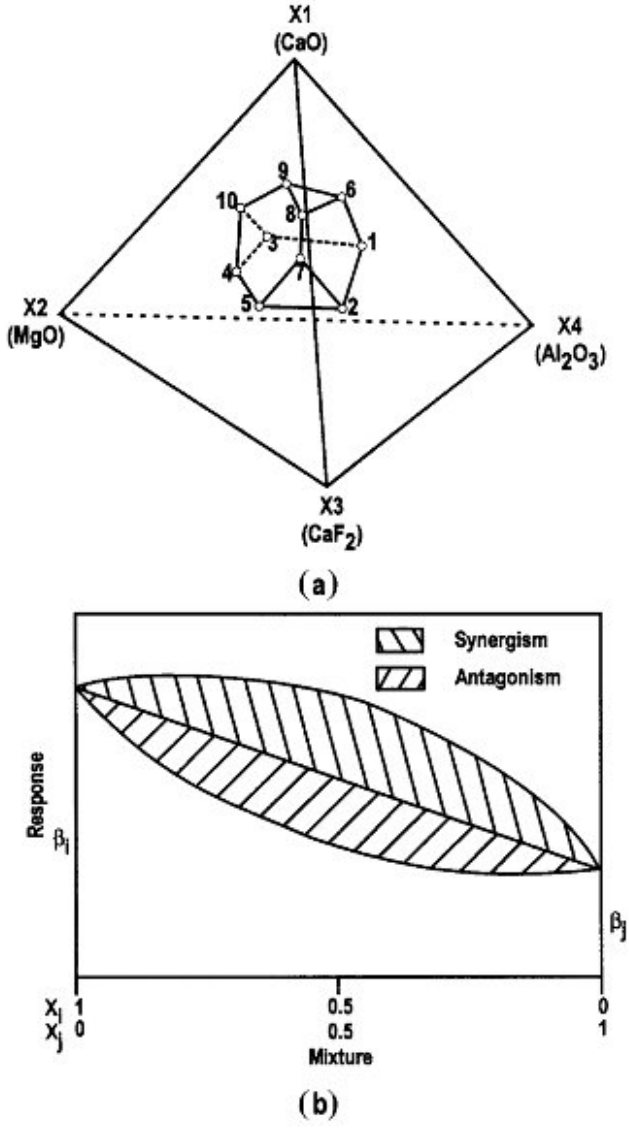

FIGURE 2.—(a) The constrained factor space inside the tetrahedron describing the experimental space; (b) Synergism and antagonism of binary mixture.

The regression coefficients β_i and β_{ij} are the least-square estimates in the fitted model, and y is the response variable.

The percentage variation of a given response characteristic is measured by the term R^2, which is evaluated from the relation

$$R^2 = 1 - \frac{\text{SSE}}{\text{SST}} \tag{2}$$

where SSE is sum of square of errors, SST is total sum-of-squares.

In the present experiment a flux ingredient (x_i) has four constituents; viz., $x_1 = \text{CaO}$, $x_2 = \text{MgO}$, $x_3 = \text{CaF}_2$, and $x_4 = \text{Al}_2\text{O}_3$.

Binary Synergism and Antagonism

The concept of binary synergism and antagonism is quite different from the individual effect. The binary synergism/antagonism implies that the response (weld metal acicular ferrite content) obtained due to binary mixture is more than/less than the average of that response produced by two pure flux ingredients forming the same binary mixture. This is shown schematically in Fig. 2(b). The positive and negative sign of the coefficients $\square_i$ in Eq. (1) indicates an increase or decrease of that response variable (y) by the flux ingredients (x_i), respectively. Similarly either positive or negative sign of coefficients $\square_{ij}$ in Eq. (1), indicates binary synergistic or antagonistic effect of the flux mixture ($x_i x_j$) on the response variable.

Experimental procedure

Eighteen reagent grade agglomerated fluxes as given in Table 1 were prepared by varying the ingredients CaO, MgO, CaF_2, and Al_2O_3 as per formulations based on statistical design. Bead-on-plate weld deposits at constant current (400 amp), voltage (26 V), speed (4.65 mm/sec) and electrode extension (25 mm) were made on 100 mm × 250 mm × 18 mm low-carbon steel plate with each of the fluxes using 3.15 mm-diameter low-carbon steel filler wire in the SAW process.

Chemical Composition Analysis

Chemical constituents such as carbon, manganese, silicon, sulfur, phosphorous, and nickel of the base metal, filler wire and weld metal were analyzed using an optical emission spectrometer (OES) operated by Quantovac method, manufactured by Jarell As. Atom Comp. (Model 750, Cat No. 96-786). Oxygen and nitrogen contents were measured using a Leco interstitial analyzer. Cylindrical machined samples of 3 mm diameter and 9 mm length were used for this purpose. The chemical compositions of filler wire, base metal and weld metal samples are given separately in Table 2.

Table 1.—Design matrix of flux used in submerged arc welding.

Sample No.	Mixture variables composition			
	CaO (wt%)	MgO (wt%)	CaF_2 (wt%)	Al_2O_3 (wt%)
P1	15.00	15.00	10.00	40.00
P2	15.00	15.00	40.00	10.00
P3	15.00	32.40	10.00	22.60
P4	15.00	17.00	40.00	8.00
P5	15.00	32.40	24.60	8.00
P6	35.00	15.00	10.00	20.00
P7	17.00	15.00	40.00	8.00
P8	35.00	15.00	22.00	8.00
P9	29.60	32.40	10.00	8.00
P10	35.00	27.00	10.00	8.00
P11	24.43	23.14	24.43	8.00
P12	15.67	15.67	40.00	8.66
P13	25.92	24.36	10.0	19.72
P14	23.40	15.00	24.40	17.20
P15	19.87	32.40	14.86	12.87
P16	15.00	22.36	24.92	17.72
P17	35.00	19.00	14.00	12.00
P18	22.67	21.63	21.63	14.07

Other additions to eighteen nos. of flux samples Wt% SiO_2 = 10.0 Wt%; Fe-Mn = 4.0 Wt%; Bentonite = 2.0; Wt% Fe-Si = 3.0 Wt%; Ni-Powder = 1.0.

Microscopic Examination

Each of the eighteen samples were cut transversely to the weld direction and prepared for microscopic studies on the weld metal zone. Samples were examined first under optical microscope, and various microstructural constituents were identified. Quantitative measurement of the microstructural constituents was performed by conventional two-dimensional point counting using an ELECO automatic point counter. The results are given in Table 3.

Evaluation of Weld Metal Mechanical Properties

Tensile and Charpy impact test samples were prepared as per dimensions specified in ASTM E8M [26] and ASTM E23 [27], respectively. Tensile tests were carried out on weld metal samples using an Instron Universal testing machine (Model 850, capacity 100 KN) at a cross head speed of 0.01 mm/s and a strain rate of 0.05 mm/sec. Impact toughness of each of the eighteen weld metal samples was evaluated by conducting Charpy "V" notch impact tests at −20°C. Hardness testing on weld metal samples was done using a Vickers hardness testing machine using a 30 kg load and 136° diagonal pyramid indenter on polished and flat samples. The weld metal mechanical properties such as yield strength (YS), ultimate tensile strength (UTS), elongation percentage (%El), impact toughness and Vickers hardness (VHN) are given in Table 4.

Scanning Electron Microscopic Study

Fractured surfaces of tensile tested and Charpy impact tested samples were examined in a scanning electron microscope (SEM; Hi-tech S-415A; operated at 20 KV) at both high and low magnification.

Results

Development of Prediction Equations for Weld Metal Mechanical Properties

Using experimentally determined weld metal mechanical properties as given in Table 4, adequate quadratic regression models in canonical form were developed for the weld metal mechanical properties (viz., YS, UTS, %El, impact toughness and VHN) as a function of wt% of flux ingredients (CaO, MgO, CaF_2, and Al_2O_3) using the model of constrained statistical mixture designs. Predictors are individual flux ingredients, i.e., CaO, MgO, $CaF_2 \cdot Al_2O_3$, and their binary mixtures, i.e., $CaO \cdot MgO$, $CaO \cdot CaF_2$, $CaO \cdot Al_2O_3$, $MgO \cdot CaF_2$, $MgO \cdot Al_2O_3$, and $CaF_2 \cdot Al_2O_3$. The prediction equations developed are as follows:

$$\text{Yield strength (YS; in MPa)} = -12.1431\ \text{CaO} + 16.1571\ \text{MgO} + 2.5666\ \text{CaF}_2 - 2.2240\ \text{Al}_2\text{O}_3 + 0.0878\ \text{CaO} \cdot \text{MgO} + 0.5069\ \text{CaO}$$

TABLE 2.—Chemical composition of base metal, filler wire and eighteen weld metal samples.

Sample No.	Carbon (wt%)	Manganese (wt%)	Silicon (wt%)	Sulfur (wt%)	Phosphorous (wt%)	Nickel (wt%)	Oxygen (ppm)	Nitrogen (ppm)
Base metal	0.22	0.77	0.25	0.03	0.02	Nil	350	50
Filler wire	0.10	0.56	0.05	0.02	0.01	Nil	380	60
				Weld metal samples				
No. P1	0.070	0.560	0.340	0.042	0.025	0.21	560	92
No. P2	0.070	0.520	0.210	0.042	0.028	0.11	570	95
No. P3	0.070	0.620	0.280	0.040	0.025	0.20	520	103
No. P4	0.060	0.470	0.170	0.034	0.023	0.17	500	86
No. P5	0.068	0.600	0.248	0.044	0.024	0.27	530	86
No. P6	0.098	0.670	0.229	0.028	0.021	0.24	380	36
No. P7	0.072	0.488	0.270	0.040	0.026	0.32	490	38
No. P8	0.070	0.580	0.200	0.028	0.022	0.29	480	22
No. P9	0.068	0.690	0.260	0.027	0.023	0.23	330	31
No. P10	0.063	0.540	0.193	0.034	0.022	0.31	480	39
No. P11	0.073	0.700	0.120	0.021	0.050	0.50	300	32
No. P12	0.095	0.601	0.150	0.037	0.070	0.34	350	43
No. P13	0.084	0.620	0.160	0.016	0.032	0.30	320	52
No. P14	0.089	0.748	0.258	0.031	0.077	0.78	300	36
No. P15	0.094	0.800	0.370	0.020	0.046	0.59	320	38
No. P16	0.061	0.507	0.200	0.024	0.025	0.05	600	76
No. P17	0.082	0.595	0.273	0.015	0.045	0.33	470	45
No. P18	0.058	0.517	0.160	0.023	0.052	0.29	540	101

$$\cdot CaF_2 + 0.6429\ CaO \cdot Al_2O_3 - 0.3743\ MgO \cdot CaF_2 - 0.2713\ MgO \cdot Al_2O_3 - 0.0063\ CaF_2 \cdot Al_2O_3 \quad (3)$$

Ultimate tensile strength (UTS; in MPa)

$$= -7.95374\ CaO + 20.16304\ MgO + 4.24123\ CaF_2 + 6.74286\ Al_2O_3 - 0.02189\ CaO \cdot MgO + 0.48070\ CaO \cdot CaF_2 + 0.50277\ CaO \cdot Al_2O_3 - 0.38560\ MgO \cdot CaF_2 - 0.48676\ MgO \cdot Al_2O_3 - 0.12777\ CaF_2 \cdot Al_2O_3 \quad (4)$$

Percent elongation (%)

$$= 0.254828\ CaO + 0.321535\ MgO + 0.143739\ CaF_2 + 0.832866\ Al_2O_3 - 0.002358\ CaO \cdot MgO + 0.008743\ CaO \cdot CaF_2 - 0.002561\ CaO \cdot Al_2O_3 + 0.006140\ MgO \cdot CaF_2 - 0.013905\ MgO \cdot Al_2O_3 - 0.027976\ CaF_2 \cdot Al_2O_3 \quad (5)$$

Charpy impact toughness at −20°C (in joules)

$$= -3.31038\ CaO + 0.62389\ MgO - 0.26209\ CaF_2 - 0.84441\ Al_2O_3 + 0.06680\ CaO \cdot MgO$$

TABLE 3.—Microstructure content of eighteen weld metal samples.*

Sample No.	Microstructure (%)				
	GBF	SPF	PF	AF	FAS
P1	37	19	27	13	4
P2	38	19	27	12	4
P3	31	18	30	15	6
P4	34	17	30	14	5
P5	38	17	27	13	5
P6	29	16	24	24	7
P7	34	20	25	16	5
P8	31	16	29	19	5
P9	29	17	20	28	6
P10	31	19	29	16	5
P11	24	14	20	35	7
P12	29	15	24	26	6
P13	27	12	27	28	6
P14	22	10	25	36	7
P15	25	14	18	35	8
P16	34	21	31	10	4
P17	32	14	28	20	6
P18	33	19	28	16	4

*GBF = Grain Boundary Ferrite; SPF = Side Plate Ferrite; PF = Polygonal Ferrite; AF = Acicular Ferrite; FAS = Ferrite with aligned second phase (Upper bainite).

TABLE 4.—Mechanical properties of eighteen weld metal samples.*

Sample No.	YS (MPa)	UTS (MPa)	Percent elongation (%)	Impact toughness at −20°C (J)	Vickers hardness (VHN)
P1	254	464	24.5	8.8	160
P2	285	428	20.0	9.8	168
P3	336	446	19.2	10.5	157
P4	290	425	17.0	9.8	175
P5	308	460	24.2	7.8	161
P6	346	485	22.4	22.2	198
P7	298	431	19.7	13.7	165
P8	305	458	24.0	14.4	164
P9	346	455	20.0	16.7	157
P10	316	456	23.2	14.7	175
P11	382	474	19.6	26.0	184
P12	326	455	17.8	15.8	157
P13	337	472	21.7	23.5	170
P14	361	496	17.6	25.5	198
P15	397	535	20.0	24.1	208
P16	286	385	13.4	9.1	152
P17	294	450	22.2	14.2	164
P18	285	435	25.9	11.6	153

*YS = Yield strength; UTS = Ultimate tensile strength.

TABLE 5.—Predominant effect of flux ingredients and their binary mixtures on weld metal mechanical properties and Mn/Si value.

	Predominant effects			
	Pure flux ingredient		Binary mixtures of flux ingredient	
(Response characteristics)	Increase	Decrease	Synergism	Antagonism
Yield strength (YS) (MPa)	MgO, CaF_2	CaO	CaO-CaF_2, CaO-Al_2O_3	MgO-CaF_2 MgO-Al_2O_3
Ultimate tensile strength (UTS) (MPa)	MgO, CaF_2, Al_2O_3	CaO	CaO-CaF_2, CaO-Al_2O_3	MgO-CaF_2, MgO-Al_2O_3, CaF_2-Al_2O_3
Elongation percent (%)	Al_2O_3	—	—	CaF_2-Al_2O_3
Impact toughness at −20°C (J)	—	CaO, Al_2O_3	CaO-MgO, CaO-CaF_2, CaO-Al_2O_3	MgO-CaF_2
Vickers hardness (VHN)	MgO, CaF_2	—	CaO-CaF_2, CaO-Al_2O_3	MgO-CaF_2 MgO-Al_2O_3
Mn/Si value	—	CaO	CaO-MgO	—

$$+ 0.10098\ CaO \cdot CaF_2 + 0.12913\ CaO \cdot Al_2O_3 - 0.03063\ MgO \cdot CaF_2 - 0.02394\ MgO \cdot Al_2O_3 - 0.00737\ CaF_2 \cdot Al_2O_3 \quad (6)$$

$$\text{Vickers Hardness (VHN)} = -2.34444\ CaO + 7.64144\ MgO + 1.90546\ CaF_2 + 0.57330\ Al_2O_3 - 0.03336\ CaO \cdot MgO + 0.13376\ CaO \cdot CaF_2 + 0.24826\ CaO \cdot Al_2O_3 - 0.13902\ MgO \cdot CaF_2 - 0.17757\ MgO \cdot Al_2O_3 + 0.00903\ CaF_2 \cdot Al_2O_3 \quad (7)$$

The model summary, i.e., significant level, standard error, "t" statistic, confidence interval for each predictor, text of whole mixture model and ANOVA for each response characteristic (Eqs. (3–7)) are given in Appendix 1.

The predominant effect of individual flux ingredients (increase or decrease) and their binary mixture (either synergism or antagonism) on weld metal mechanical properties were determined by considering their significant values (t and P) at 95% confidence level as given in Appendix 1, and corresponding prediction Eqs. (3–7). The results are summarized in Table 5. Since the prediction results of weld metal percent elongation (%El) and Vickers hardness (VHN) are not good fits, as evident from their R^2 values (Appendix 1), these two responses, i.e., weld metal percentage elongation and hardness, are not considered for further discussion. Similarly to weld metal mechanical properties, the predominant effect of flux ingredients and their binary mixtures on submerged arc weld metal chemistry and microstructural constituents were also determined by the investigators in their previous studies [11, 21] under identical experimental conditions by developing prediction equations for weld metal chemical composition and microstructural constituents.

DISCUSSION

Fluxes in the SAW process control the weld metal mechanical properties by their influence upon the chemical composition and microstructure of the weld metal. The weld metal YS, UTS and impact toughness increase with an increase in alloying elements, viz., carbon (up to 0.10 wt%), manganese (up to 1.5 wt%), silicon (up to 0.5 wt%) and nickel (up to 3.5 wt%) by various mechanisms such as (1) solid solution hardening, (2) grain refinement and (3) refinement of micro structure [28–31]. Oxygen can affect YS and UTS by its (1) control over weld metal microstructure through the formation of inclusions [13–16] and (2) its controlling effect on elements C, Mn and Si during slag metal reaction [30–32]. The basic requirement of improved toughness in low-alloy steel weld metal is associated with the amount of acicular ferrite in the microstructure [12–16]. Intragranularly formed randomly oriented short needles of acicular ferrite as shown in Fig. 3 were observed in sample P14 which contains maximum acicular ferrite content (36%) in the present study. Furthermore, the weld metal Mn/Si ratio should be high, and S level should be low in order to obtain high impact toughness [33].

Effect of Flux Ingredients on Weld Metal Chemical Composition

A detailed investigation was carried out by the authors to determine the effect of flux ingredients on weld metal chemical composition under identical working conditions [11]. The prediction equations developed for weld metal chemical constituents in terms of flux ingredients are given in Appendix 2. The predominant effects of flux

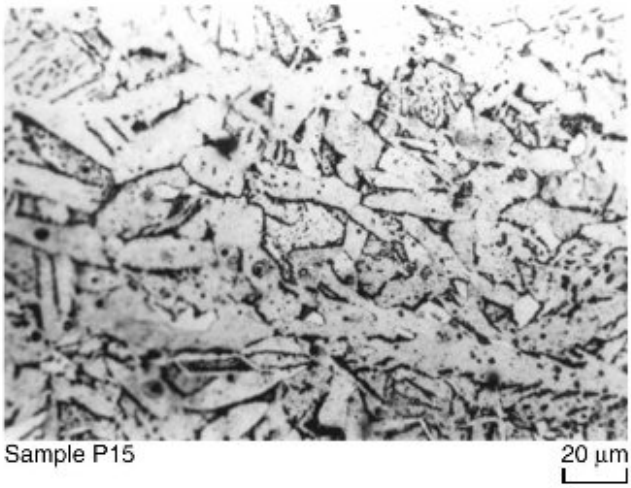

FIGURE 3.—Optical Microstructure of Sample P14 showing randomly dispersed needles of acicular ferrite (AF). Grain boundary ferrites are also seen in the microstructure.

TABLE 6.—Predominant effect of flux ingredients and their binary mixtures on weld metal chemical composition [11] and microstructural constituents [21].*

	Predominant effects			
	Pure flux ingredient		Binary mixtures of flux ingredient	
(Response characteristics)	Increase	Decrease	Synergism	Antagonism
Oxygen (ppm)	CaO, CaF_2, Al_2O_3	—	MgO-CaF_2, MgO-Al_2O_3, CaF_2-Al_2O_3	CaO-MgO, CaO-CaF_2, CaO-Al_2O_3
Manganese (wt%)	MgO	CaO	CaO-CaF_2, CaO-Al_2O_3	MgO-CaF_2, MgO-Al_2O_3
Silicon (wt%)	CaO, MgO, CaF_2, Al_2O_3	—	—	CaO-MgO, MgO-CaF_2, MgO-Al_2O_3
Sulfur (wt%)	CaO, MgO, CaF_2, Al_2O_3	—	—	CaO-MgO, CaO-CaF_2, CaO-Al_2O_3, MgO-Al_2O_3
Nickel (wt%)	MgO	CaO, CaF_2,	CaO-CaF_2, CaO-Al_2O_3	MgO-CaF_2, MgO-Al_2O_3
Carbon (wt%)	MgO-CaF_2	—	CaO-CaF_2, CaO-Al_2O_3	CaO-MgO, MgO-CaF_2, MgO-Al_2O_3
GBF	CaO, Al_2O_3	—	—	CaO-CaF_2, CaO-Al_2O_3
SPF	—	—	—	CaO-Al_2O_3
PF	CaO	—	MgO-Al_2O_3	CaO-CaF_2, CaO-Al_2O_3
AF	—	CaO	CaO-CaF_2, CaO-Al_2O_3	—
FAS	—	—	CaO-Al_2O_3	—

*Microstructural constituents: GBF = Grain Boundary Ferrite; SPF = Side Plate Ferrite; PF = Polygonal Ferrite; AF = Acicular Ferrite; FAS = Ferrite with Aligned Second Phase (Upper Bainite).

ingredients and their binary mixture on weld metal chemical constituents are given in Table 6. Flux ingredients control the weld metal chemical composition by combined effects of several mechanism; viz., slag metal reactions, viscosity of flux, atmospheric entrainment in the molten weld pool, electrochemical reactions, formation of complex compounds, thermodynamics as well as kinetics of slag metal reaction, weld bead geometry, and so on. The mechanisms pertaining to each of the chemical constituents have been elaborated in Kanjilal et al. [11].

Effect of Flux Ingredients on Weld Metal Microstructural Constituents

Under similar experimental conditions, prediction equations were also developed for weld metal microstructural constituents in terms of flux ingredients [21]. The details of the equations are given in Appendix 2. The predominant effect of flux ingredients and their binary mixtures on weld metal microstructural constituents are also included in Table 6. The formation of microstructural constituents depends on weld metal chemical composition and inclusion characteristics when welds are performed using constant welding parameters [34]. Weld bead geometry also influences formation of microstructure constituents, especially acicular ferrite [34].

Weld Metal Yield Strength

It is apparent from the results of Table 5 that flux ingredient CaO decreases weld metal yield strength, but two ingredients, i.e., MgO and CaF_2, increase weld metal yield strength. Flux mixtures $CaO \cdot CaF_2$ and $CaO \cdot Al_2O_3$ have binary synergistic (increasing) effects on weld metal yield strength, whereas mixtures $MgO \cdot CaF_2$ and $MgO \cdot Al_2O_3$ have binary antagonistic (decreasing) effects on YS (Table 6).

The decreasing effect on YS by CaO may be expected since CaO increases weld metal oxygen as well as decreases weld metal manganese and nickel content. Similarly, the increasing effect on YS by MgO is not unexpected, since MgO increases weld metal manganese and nickel content in weld metal. The binary synergism (increasing effect) of $CaO \cdot CaF_2$ and $CaO \cdot Al_2O_3$ mixtures on YS could also be due to (1) binary synergism of $CaO \cdot CaF_2$ and $CaO \cdot Al_2O_3$ mixtures on weld metal manganese and nickel content, (2) binary synergism of $CaO \cdot Al_2O_3$ mixture on weld metal carbon content, and/or (3) binary antagonism of $CaO \cdot CaF_2$ and $CaO \cdot Al_2O_3$ mixtures on weld metal oxygen content (Table 6). Again, binary antagonism (decreasing effect) of $MgO \cdot CaF_2$ and $MgO \cdot Al_2O_3$ mixtures on YS could be due to (1) binary synergism (increasing effect) of $MgO \cdot CaF_2$ and $MgO \cdot Al_2O_3$ mixtures on oxygen content and/or (2) binary antagonism (decreasing effect) of $MgO \cdot CaF_2$ and $MgO \cdot Al_2O_3$ mixtures on manganese, silicon, nickel and carbon content (Table 6).

The increase of weld metal YS with hardenability measuring expression, i.e., carbon equivalent (Table 7), as shown in Fig. 4(a) indicates the effect of chemical constituents such as C, Mn, Ni on weld metal YS. Similarly the decrease of YS with oxygen content, as shown in Fig. 5(a) also indicates the effect of oxygen content, or, more precisely, weld metal inclusion content, on the YS values. It has been already reported that inclusion volume fraction increases with increasing oxygen content, which ultimately coarsens weld metal microstructure [13]. However, it is observable in Figs. 4(a) and 5(a) that there are variations of YS even at a fixed value of carbon equivalent (CE) and oxygen content, which probably indicate that other mechanisms, in addition to CE and oxygen content, are involved in controlling weld metal YS. For example, sample P15 shows higher YS (397 MPa) compared to sample P13 (337 MPa) at an oxygen content (~320 ppm) of weld metal. It is interesting to note from Table 6 that sample P15 has higher CE (0.267) than sample P13 (0.207). Furthermore, they also differ in microstructural constituents; in particular, the acicular ferrite content, which is significantly greater in sample P15 (35%) than sample P13 (28%). Therefore, the higher YS of sample Pl5 is attributed to the higher CE, which probably caused the higher AF content in the microstructure. Similarly, sample P11 shows higher YS (382 MPa) than sample P6 (346 MPa) at a given CE (0.225); and they differ in oxygen content (300 ppm for

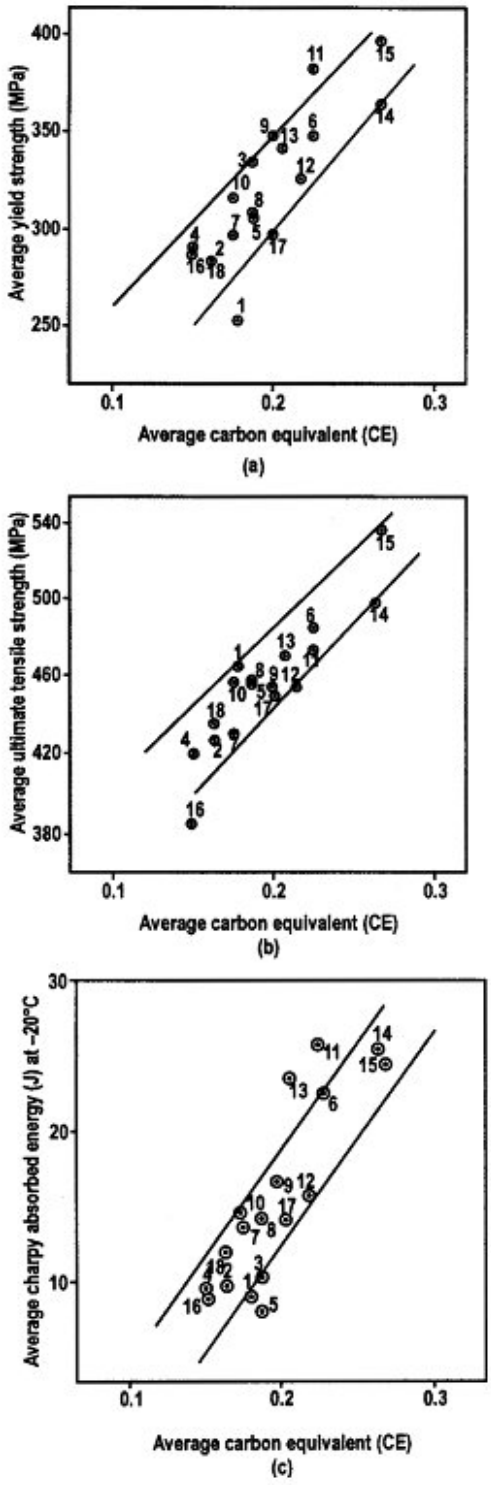

FIGURE 4.—Effect of carbon equivalent (CE) on weld metal mechanical properties for different samples: (a) yield strength (YS), (b) ultimate tensile strength (UTS), and (c) charpy impact toughness at −20°C.

P11 and 380 ppm for P6) and microstructural constituents, in particular AF content (24% for sample P6 and 35% for P11). Therefore, for a given CE value, the higher YS in sample P11 is associated with lower oxygen content and more AF content.

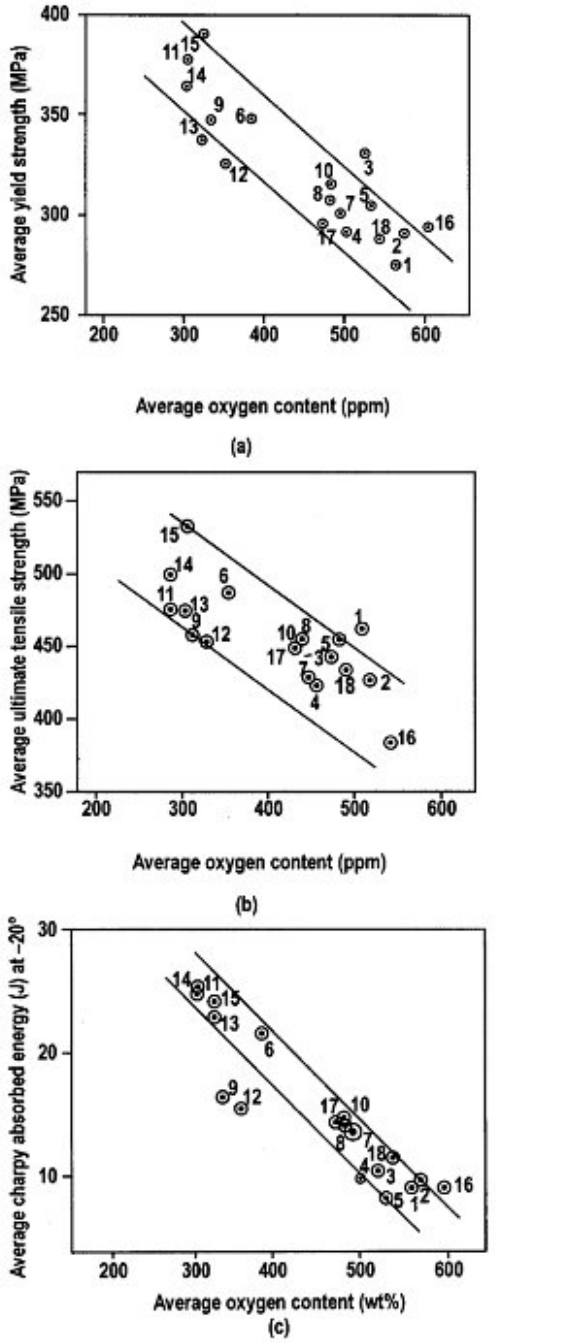

FIGURE 5.—Effect of oxygen content on weld metal mechanical properties for different samples: (a) yield strength (YS), (b) ultimate tensile strength (UTS), and (c) charpy impact toughness at −20°C.

Weld Metal Ultimate Tensile Strength

CaO decreases weld metal UTS, but other flux ingredients, e.g., MgO, CaF_2, and Al_2O_3 increase UTS. Flux mixtures $CaO \cdot CaF_2$ and $CaO \cdot Al_2O_3$ have a binary synergistic (increasing) effect on weld metal UTS. However, other flux mixtures, i.e., $MgO \cdot CaF_2$, $MgO \cdot Al_2O_3$, and $CaF_2 \cdot Al_2O_3$ have a binary antagonistic (decreasing) effect on UTS (Table 6).

The increasing UTS with increase in MgO may be expected since MgO increases weld metal Mn, Si, C, and Ni content (Table 6), and these elements are found to increase UTS. Similarly, Al_2O_3 increases weld metal Si content which ultimately contributes to an increase in UTS. CaF_2 also increases weld metal Si and C content which also contribute to an increase in UTS (Table 6). The binary synergistic (increasing) effect of flux mixtures $CaO \cdot CaF_2$ and $CaO \cdot Al_2O_3$ on weld metal UTS may be explained by their (1) binary synergistic effect on weld metal Mn, Ni, and C content and (2) binary antagonistic effect on weld metal oxygen content. Similarly, the opposite effect, i.e., binary antagonistic effect of flux mixtures $MgO–CaF_2$ and $MgO–Al_2O_3$ on weld metal UTS may be explained by their (1) binary antagonistic effect on weld metal Mn, Si, Ni and C content and (2) binary synergistic effect on weld metal oxygen content (Table 6).

Weld metal UTS has also been correlated with carbon equivalent (CE), the values of which are given in Table 6. The increase of UTS with CE as shown in Fig. 4(b) clearly indicates the role of hardening elements (such as C, Mn, and Ni) on weld metal UTS. As expected, weld metal UTS decreases with the increase of oxygen content, as shown in Fig. 5(b). This is due to coarsening of the weld metal microstructure with an increase in oxygen content [14]. However, it appears from both Figs. 4(b) and 5(b) that UTS varies considerably, even at a fixed value of CE and oxygen content. These phenomena indicate that, apart from CE and oxygen, other factors may influence the weld metal UTS. For example, at a given oxygen content (320 ppm), sample P15 has higher UTS (535 MPa) than sample P13 (472 MPa). Like YS, the higher UTS of sample P15 is attributed to higher CE, which probably causes higher AF content. Furthermore, the presence of some pearlite in between GBF in sample P15 as observed in a TEM micrograph (Fig. 6) may increase the UTS value. Similarly, sample P13 shows a higher UTS (472 MPa) than sample P17 (450 MPa) at a given CE (0.202), and they differ in oxygen content (320 ppm for P13 and 470 ppm for P17) and microstructural constituents (Table 3), in particular AF (28% for P13 and 20% for P17) and GBF content (27% for P13 and 32% for P17). Therefore, for a given CE value, higher UTS in sample P13 is associated with lower oxygen content and more AF (8% more) as well as lower GBF content (5% less).

On the other hand, it is interesting to note that samples P15 and P14, having almost the same CE value of 0.266 and level of oxygen (320 ppm), as given in Table 2, showed different UTS values. Higher UTS in sample P15 than P14 could be due to lower sulfur and phosphorous content (Table 2). Sulfur and phosphorous usually promote metallurgical stress concentration and provide sites for the nucleation of microvoids during tensile loading. Relatively larger microvoids of sample P14 [Fig. 7(a)] compared to sample P15 (Fig. 7(b)) clearly indicate the role of sulfur in fracture under tensile loading.

Weld Metal Toughness

Results in Table 5 show that flux ingredients CaO and Al_2O_3 decrease weld metal Charpy impact toughness. Flux

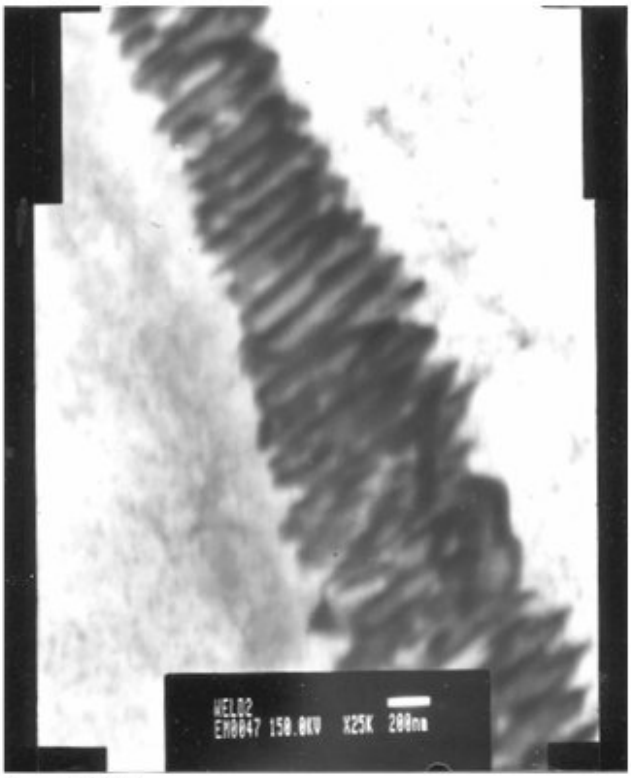

Sample P15

FIGURE 6.—TEM micrograph showing nucleation of some pearlite in between large veins of grain boundary ferrite.

mixtures $CaO \cdot CaF_2$, $CaO \cdot Al_2O_3$ and $CaO \cdot MgO$ have a binary synergistic (increasing) effect on weld metal impact toughness. The effect of $CaO \cdot MgO$ is much less in comparison with other mixtures, e.g., $CaO \cdot CaF_2$ and $CaO \cdot Al_2O_3$, as is evident from their respective coefficients of estimate in the prediction equations of weld metal Charpy impact toughness (Eq. (7)). However, the flux mixture $MgO \cdot CaF_2$ has a binary antagonistic (decreasing) effect on weld metal Charpy impact toughness (Table 5).

The decrease in impact toughness with increasing in CaO in the flux may be expected because CaO increases weld metal oxygen content (Table 6) which minimizes AF content in the microstructure [14–16]. On the other hand, the binary synergism (increasing effect) of $CaO \cdot CaF_2$ and $CaO \cdot Al_2O_3$ mixture on weld metal toughness could be attributed to (1) binary synergism of $CaO \cdot CaF_2$ and $CaO \cdot Al_2O_3$ mixtures on weld metal manganese, nickel and carbon content and (2) binary antagonism (decreasing effect) of $CaO \cdot CaF_2$ and $CaO \cdot Al_2O_3$ mixtures on weld metal oxygen content. The probable reasons for these observations have been discussed in previous work [11]. Furthermore, both of these flux mixtures, i.e., $CaO \cdot CaF_2$ and $CaO \cdot Al_2O_3$ have a binary synergistic (increasing) effect on weld metal acicular ferrite content (Table 6), which always improves weld metal Charpy impact toughness [12–16]. The binary antagonism (decreasing effect) of the $MgO \cdot CaF_2$ flux mixture on Charpy impact toughness may be attributed to its binary synergism (increasing effect) on weld metal oxygen

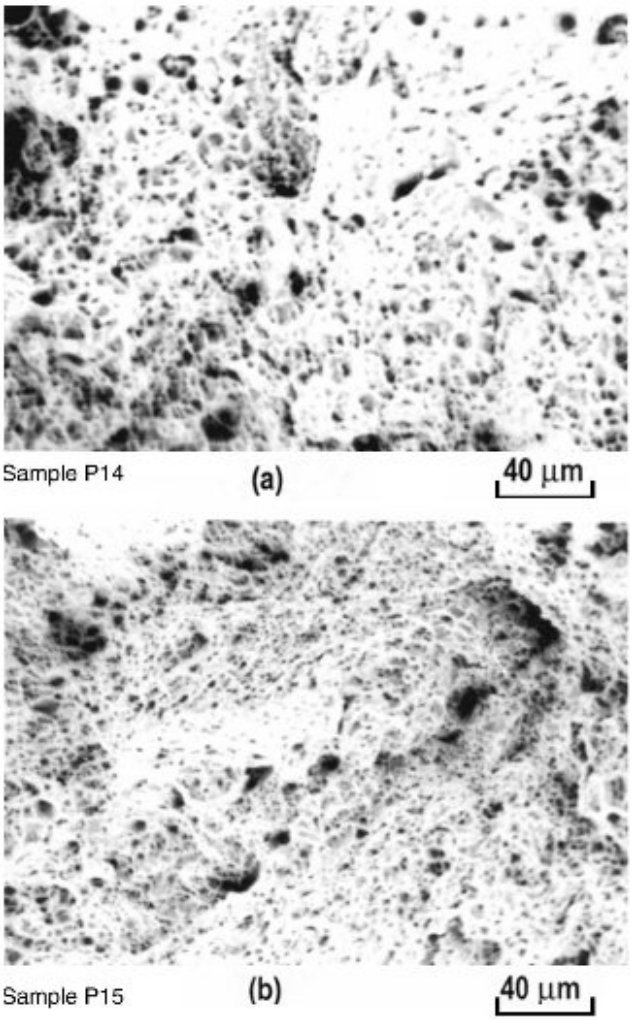

FIGURE 7.—SEM micro photograph of tensile fractured samples: (a) P14 showing fine dimples alongwith few large voids, (b) P15 showing fine dimples alongwith small voids.

content and binary antagonism on weld metal Mn, Si, Ni, and C content (Table 6). The increase in oxygen content is directly associated with the increase in volume fraction of inclusions and consequent decrease in acicular ferrite content [13–16]. Furthermore, $MgO \cdot CaF_2$ has a binary antagonistic (decreasing effect) effect on acicular ferrite content (Table 6) which decreases Charpy impact toughness.

Although the weld metal toughness increases with increasing carbon equivalent (CE) and decreases with the greater oxygen content, as shown in Figs. 4(c) and 5(c), respectively, the variation of toughness, even at a fixed value of CE and oxygen content, probably indicates that some other factors in addition to CE and oxygen content are responsible for controlling weld metal toughness. The weld metal of sample P11 has maximum toughness (26 J) although it has lower carbon equivalent (CE 0.225) than sample P15 (CE 0.266). Both samples P11 and P15 have the same percentage of microstructural constituent acicular ferrite. It therefore appears that the higher oxygen content (20 ppm more) in P15 over P11 is responsible for a slight

TABLE 7.—Weld metal carbon equivalent (CE) and Mn to Si ratio (Mn/Si) for eighteen samples.*

Sample No.	CE%	$\frac{Mn}{Si}$
P1	0.177	1.647
P2	0.164	2.476
P3	0.187	2.214
P4	0.149	2.765
P5	0.186	2.419
P6	0.225	2.926
P7	0.174	1.807
P8	0.186	2.90
P9	0.198	2.654
P10	0.173	2.798
P11	0.224	5.833
P12	0.217	4.006
P13	0.207	3.875
P14	0.266	2.899
P15	0.267	2.162
P16	0.148	2.535
P17	0.202	2.179
P18	0.164	3.231

*Carbon equivalent (CE) = wt% C + $\frac{wt\%Mn}{6}$ + $\frac{wt\%Ni}{15}$.

decrease in impact toughness in P15(24.1 J) over P11 (26 J). Furthermore, at the same CE value (0.266) a slight increase in Charpy impact toughness in P14 (25.5 J) over P15 (24.1 J) has been observed. Table 3 shows that sample P14 contains slightly more AF and PF content, and less GBF, SPF and FAS content, than P15. Again, the Mn:Si ratio in P14 (2.899) is slightly higher than P15 (2.162) as given in Table 7, both of which are probably responsible for a slight improvement in the impact toughness of P14 over sample P15.

It is also observable from Table 4 that sample P13 has better toughness (23.5 J) as compared with P9 (16.7 J), although both of these samples have almost the same CE value 0.20 (Table 7) and oxygen content (P13 320 ppm and P9 330 ppm). Although P13 and P9 have the same AF content (28%) as given in Table 3, SPF content is 5% lower in P13 than P9, GBF content is 2% less in P13 than P9 and PF content is 7% more in P13 than P9. Furthermore, the Mn/Si ratio (Table 6) in P13 (3.875) is more than that of P9 (2.654). Therefore, it may be stated that an increase in PF, a decrease in SPF and GBF and higher Mn/Si ratio (Table 6) may be responsible for higher toughness in sample P13 than P9, even at the same AF content. Differing in impact toughness between P13 and P9 is also reflected in the SEM fractograph as sample P13 [Fig. 8(a)] shows more (ductile fracture) of MVC as compared to fracture in sample P9 [Fig. 8(b)].

It is also important to note that sample P6 having higher CE (0.225) and higher oxygen content (380 ppm) than sample P9 and having lower CE (0.198) and lower oxygen content of 330 ppm has a higher toughness (22.2 J) than P9 (16.7 J) as given in Table 4. Furthermore, sample P6 has lower AF content (24%) than P9 (28%), but greater PF content (24%) than that of sample P9 (20%). The improved impact toughness of sample P6 over sample P9, despite lower AF content, may result from a higher Mn/Si ratio of P6 (2.926) than P9 (2.645). Furthermore, the decrease in impact toughness due to a decrease in AF content could

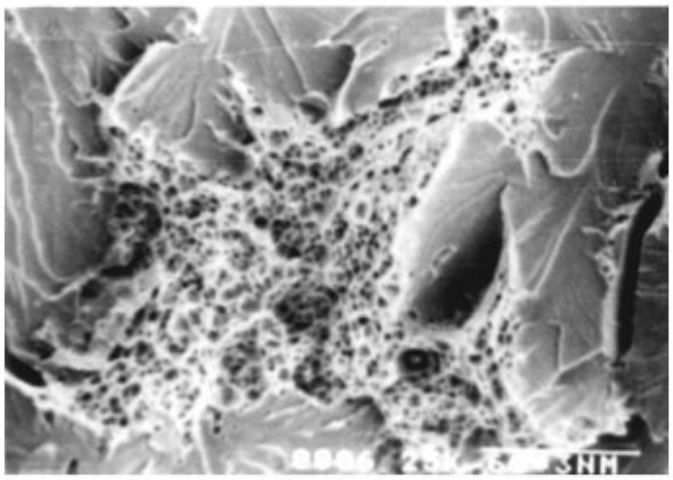

Sample P13 a

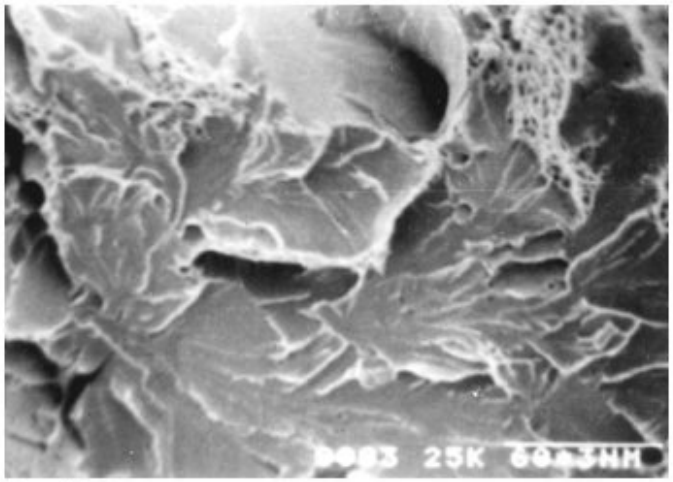

Sample P9 b

FIGURE 8.—(a) SEM fractograph of charpy impact test samples at the root of notch showing ductile brittle transition zone; (b) SEM fractograph of charpy impact test samples at the root of the notch showing brittle fracture by Quasi cleavage type failure.

TABLE 8.—Randomly designed submerged arc flux composition.

	Mixture variables composition				Constant composition
Sample No.	CaO (wt%)	MgO (wt%)	CaF_2 (wt%)	Al_2O_3 (wt%)	SiO_2 (wt%)
T1	17	20	30	13	10
T2	30	15	15	20	10
T3	25	30	15	10	10
T4	15	25	10	30	10
T5	20	28	12	20	10
T6	23	27	15	15	10
T7	19	18	11	32	10
T8	16	17	25	22	10

N.B.: Other additions to eight nos. of flux samples: Fe-Mn = 4.0 wt%, Fe-Si = 3.0 wt%, Ni-Powder = 1.0 wt%, Bentonite = 2.0 wt%.

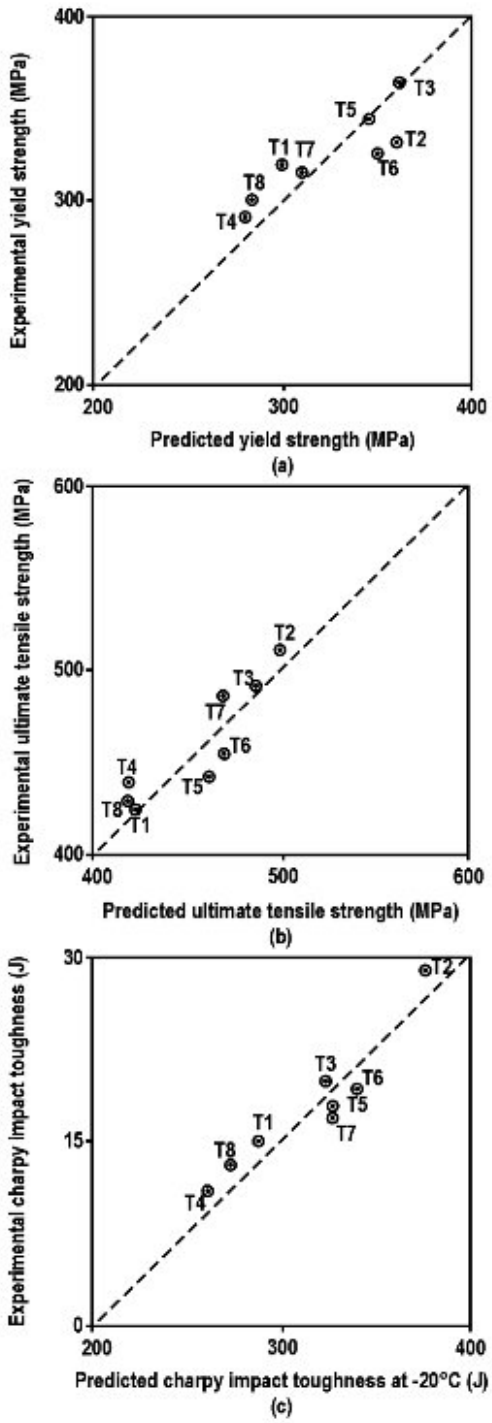

FIGURE 9.—Predicted results for weld metal mechanical properties (a) yield strength, (b) ultimate tensile strength, and (c) charpy impact toughness at –20°C.

be compensated, at least to some extent, by increasing the polygonal ferrite content.

Therefore, it appears that weld metal toughness is dependent on several factors, such as carbon equivalent (CE), oxygen content, microstructural constituents and Mn/Si ratio, which interact in a complex manner resulting in final weld metal impact toughness.

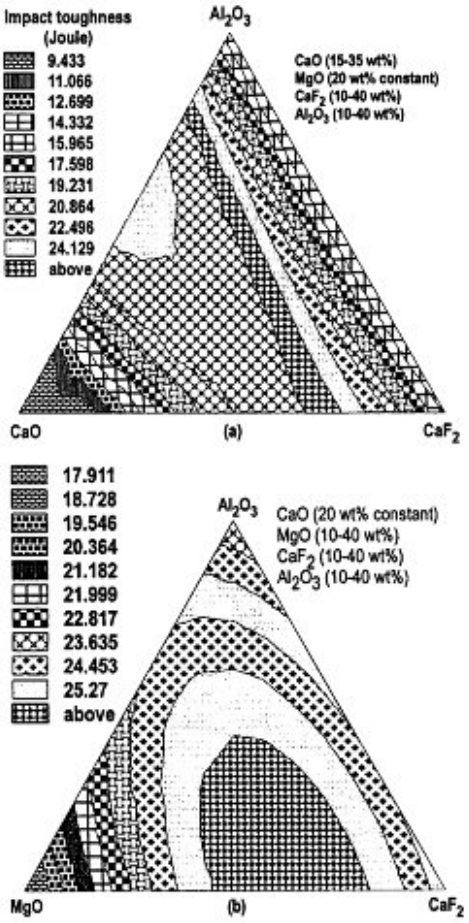

FIGURE 10.—Fitted response surface (Eqn. No. 6) contour for weld metal impact toughness at –20°C (Joule) for two different flux systems: (a) MgO constant (20 wt%) and (b) CaO constant (20 wt%).

Adequacy of the Developed Prediction Equation

The adequacy of the prediction equation developed by the regression model for weld metal mechanical properties was checked by performing SAW experiments using randomly designed fluxes. The randomly designed flux compositions are given in Table 8. The responses which were studied are weld metal mechanical properties: (1) yield strength, (2) ultimate tensile strength, and (3) Charpy impact toughness. The comparison between experimentally determined and predicted values of the responses is shown graphically in Fig. 9. We observed from these figures that there is reasonably good agreement between the experimental and predicted results. Therefore, it can be concluded that the prediction model is quite adequate in describing submerged arc weld metal mechanical properties.

Contour Plots of the Estimated Responses

The iso-response contour plots for selected responses such as weld metal impact toughness at −20°C were developed as an example. These are shown in Fig. 10. The shade in each of these iso-response contour plots represents the value of the response (impact toughness) which may be achieved with different combinations of flux ingredients in the present set of experiments.

CONCLUSIONS

The weld metal responses such as mechanical properties in submerged arc welding have been predicted in terms of flux ingredients by developing regression equations with the help of statistical experiments for mixture design. Both the individual flux ingredients CaO, MgO, CaF_2, and Al_2O_3, and their binary flux mixtures are shown to be important for weld metal properties. Generally good agreement is observed between predicted and observed results of responses. The conclusions drawn from the present studies on submerged arc welding at fixed levels of welding parameters are summarized below for each of the responses.

(i) Flux ingredient CaO improves the mechanical properties, viz., yield strength, ultimate tensile strength and Charpy impact toughness at 20°C by virtue of its interaction with both CaF_2 and Al_2O_3.
(ii) Flux ingredient MgO, on the other hand, improves the mechanical properties as an individual ingredient.
(iii) Interaction of MgO with CaF_2 and Al_2O_3 is detrimental to mechanical properties in general.
(iv) In addition to acicular ferrite, Mn:Si ratio also has an important effect on Charpy impact toughness at −20°C.

APPENDIX 1

"*t*" value and significant level (P) of each predictor, text of whole mixture model for the responses of weld metal mechanical properties.

	Responses									
	Yield strength		Ultimate tensile strength		Elongation percent		Impact toughness		Vickers hardness	
Predictors	*t*	Sig. (P)	*t*	Sig. (P)	*t*	Sig. (P)	*t*	Sig. (P)	*t*	Sig. (P)
CaO	−4.28488*	.000065*	−3.38209*	.001250*	1.05368	.296118	−8.57894*	.000000*	−1.58440	.118191
MgO	4.13200*	.000110*	6.21381*	.000000*	.96356	.339009	1.17180	.245762	3.74273*	.000400*
CaF_2	2.22375*	.029817*	4.42814*	.000039*	1.45933	.149523	−1.66769	.100421	3.16184*	.002427*
Al_2O_3	−1.54195	.128174	5.63348*	.000000*	6.76640*	.000000*	−4.29963*	.000062*	.76125	.449394
CaO · MgO	.75568	.452700	−.22699	.821179	−.23778	.812836	4.22121*	.000081*	−.54972	.584485
CaO · CaF_2	6.13372*	.000000*	7.00984*	.000000*	1.23972	.219750	8.97491*	.000000*	3.10016*	.002908*
MgO · CaF_2	−3.53116*	.000787*	−4.38375*	.000046*	.67872	.499841	−2.12255*	.037793*	−2.51191*	.014626*
CaO · Al_2O_3	7.14065*	.000000*	6.72963*	.000000*	−.33335	.739993	10.53415*	.000000*	5.28135*	.000002*
MgO · Al_2O_3	−2.41039*	.018915*	−5.21234*	.000002*	−1.44787	.152692	−1.56216	.123341	−3.02202*	.003647
CaF_2 · Al_2O_3	−.08475	.932736	−2.05961*	.043641*	−4.38515*	.000046*	−.72358	.472044	.23143	.817742

Text of whole mixture model.

Dependent variable responses	R^2	SS model	df model	MS model	SS residual
Yield strength (YS)	.627587	65266.94	9	7251.882	38729.67
Ultimate tensile strength (UTS)	.634413	46282.50	9	5142.500	26670.78
Elongation percent	.524947	311.6805	9	34.63116	282.0561
Impact toughness	.729963	1941.008	9	215.6676	718.0419
Vickers hardness	.415905	7518.366	9	835.3740	10558.75
	df residual	MS residual	F value	P significance	
Yield strength (YS)	62	624.6721	11.60910	.000000	
Ultimate tensile strength (UTS)	62	430.1739	11.95447	.000000	
Elongation percent	62	4.549292	7.612429	.000000	
Impact toughness	62	11.58132	18.62202	.000000	
Vickers hardness	62	170.3023	4.905241	.000057	

Appendix 2

$$\begin{aligned}\text{Oxygen } (O_2 \text{ ppm}) = {} & 63.305\ \text{CaO} - 12.420\ \text{MgO} \\ & + 6.457\ \text{CaF}_2 + 16.775\ \text{Al}_2\text{O}_3 \\ & - 0.945\ \text{CaO} \cdot \text{MgO} \\ & - 1.557\ \text{CaO} \cdot \text{CaF}_2 \\ & - 2.061\ \text{CaO} \cdot \text{Al}_2\text{O}_3 \\ & + 0.835\ \text{MgO} \cdot \text{CaF}_2 \\ & + 0.767\ \text{MgO} \cdot \text{Al}_2\text{O}_3 \\ & + 0.378\ \text{CaF}_2 \cdot \text{Al}_2\text{O}_3 \end{aligned} \quad (1)$$

$$\begin{aligned}\text{Manganese } (\text{Mn}\%) = {} & 0.0244\ \text{CaO} + 0.0590\ \text{MgO} \\ & + 0.0012\ \text{CaF}_2 + 0.0024\ \text{Al}_2\text{O}_3 \\ & - 0.0004\ \text{CaO} \cdot \text{MgO} \\ & + 0.0012\ \text{CaO} \cdot \text{CaF}_2 \\ & + 0.0013\ \text{CaO} \cdot \text{Al}_2\text{O}_3 \\ & - 0.0013\ \text{MgO} \cdot \text{CaF}_2 \\ & - 0.0014\ \text{MgO} \cdot \text{Al}_2\text{O}_3 \\ & - 0.0002\ \text{CaF}_2 \cdot \text{Al}_2\text{O}_3 \end{aligned} \quad (2)$$

$$\begin{aligned}\text{Silicon } (\text{Si}\%) = {} & 0.0107\ \text{CaO} + 0.0520\ \text{MgO} \\ & + 0.0083\ \text{CaF}_2 + 0.0128\ \text{Al}_2\text{O}_3 \\ & - 0.0011\text{CaO} \cdot \text{MgO} \\ & - 0.0001\ \text{CaO} \cdot \text{CaF}_2 \\ & - 0.00008\ \text{CaO} \cdot \text{Al}_2\text{O}_3 \\ & - 0.0012\ \text{MgO} \cdot \text{CaF}_2 \\ & - 0.0013\ \text{MgO} \cdot \text{Al}_2\text{O}_3 \\ & + 0.0002\ \text{CaF}_2 \cdot \text{Al}_2\text{O}_3 \end{aligned} \quad (3)$$

$$\begin{aligned}\text{Sulfur } (\text{S}\%) = {} & 0.00312\ \text{CaO} + 0.00471\ \text{MgO} \\ & + 0.00181\ \text{CaF}_2 + 0.00220\ \text{Al}_2\text{O}_3 \\ & - 0.00015\ \text{CaO} \cdot \text{MgO} \\ & - 0.00007\ \text{CaO} \cdot \text{CaF}_2 \\ & - 0.00008\ \text{CaO} \cdot \text{Al}_2\text{O}_3 \\ & - 0.0009\ \text{MgO} \cdot \text{CaF}_2 \\ & - 0.00011\ \text{MgO} \cdot \text{Al}_2\text{O}_3 \\ & - 0.00002\ \text{CaF}_2 \end{aligned} \quad (4)$$

$$\begin{aligned}\text{Nickel } (\text{Ni}\%) = {} & -.0776\ \text{CaO} + 0.0556\ \text{MgO} \\ & - 0.0181\ \text{CaF}_2 - 0.0058\ \text{Al}_2\text{O}_3 \\ & + 0.0006\ \text{CaO} \cdot \text{MgO} \\ & + 0.0030\ \text{CaO} \cdot \text{CaF}_2 \\ & + 0.0026\ \text{CaO} \cdot \text{Al}_2\text{O}_3 \\ & - 0.0015\ \text{MgO} \cdot \text{CaF}_2 \\ & - 0.0018\ \text{MgO} \cdot \text{Al}_2\text{O}_3 \\ & + 0.0004\ \text{CaF}_2 \cdot \text{Al}_2\text{O}_3 \end{aligned} \quad (5)$$

$$\begin{aligned}\text{Carbon } (\text{C}\%) = {} & -.00118\ \text{CaO} + 0.00656\ \text{MgO} \\ & + 0.00185\ \text{CaF}_2 \\ & + 0.00034\ \text{Al}_2\text{O}_3 \\ & - 0.00009\ \text{CaO} \cdot \text{MgO} \\ & + 0.00007\ \text{CaO} \cdot \text{CaF}_2 \\ & + 0.00017\ \text{CaO} \cdot \text{Al}_2\text{O}_3 \\ & - 0.00016\ \text{MgO} \cdot \text{CaF}_2 \\ & - 0.00013\ \text{MgO} \cdot \text{Al}_2\text{O}_3 \\ & - 0.00002\ \text{CaF}_2 \cdot \text{Al}_2\text{O}_3 \end{aligned} \quad (6)$$

$$\begin{aligned}\text{Grain Boundary Ferrite } (\text{GBF}\%) & \\ = {} & 2.6632\ \text{CaO} + 0.1473\ \text{MgO} \\ & + 0.7956\ \text{CaF}_2 + 1.2687\ \text{Al}_2\text{O}_3 \\ & - 0.0455\ \text{CaO} \cdot \text{MgO} - 0.0720\ \text{CaO} \cdot \text{CaF}_2 \\ & - 0.0752\ \text{CaO} \cdot \text{Al}_2\text{O}_3 + 0.0254\ \text{MgO} \cdot \text{CaF}_2 \\ & + 0.0029\ \text{MgO} \cdot \text{Al}_2\text{O}_3 - 0.0086\ \text{CaF}_2 \cdot \text{Al}_2\text{O}_3 \end{aligned} \quad (7)$$

Side Plate Ferrite (SPF%)

$$= 1.4496\ CaO - 0.2051\ MgO + 0.4395\ CaF_2 + 0.5953\ Al_2O_3 - 0.0145\ CaO \cdot MgO - 0.0415\ CaO \cdot CaF_2 - 0.0496\ CaO \cdot Al_2O_3 + 0.0140\ MgO \cdot CaF_2 + 0.0130\ MgO \cdot Al_2O_3 + 0.0038\ CaF_2 \cdot Al_2O_3 \quad (8)$$

Polygonal Ferrite (PF%)

$$= 2.2848\ CaO - 1.2764\ MgO + 0.3102\ CaF_2 + 0.1683\ Al_2O_3 - 0.0135\ CaO \cdot MgO - 0.0540\ CaO \cdot CaF_2 - 0.0646\ CaO \cdot Al_2O_3 + 0.0461\ MgO \cdot CaF_2 + 0.0656\ MgO \cdot Al_2O_3 + 0.0145\ CaF_2 \cdot Al_2O_3 \quad (9)$$

Acicular Ferrite (AF%)

$$= -4.8335\ CaO + 2.0808\ MgO - 0.3680\ CaF_2 - 0.6867\ Al_2O_3 + 0.0756\ CaO \cdot MgO + 0.1551\ CaO \cdot CaF_2 + 0.1701\ CaO \cdot Al_2O_3 - 0.0731\ MgO \cdot CaF_2 - 0.0721\ MgO \cdot Al_2O_3 - 0.0068\ CaF_2 \cdot Al_2O_3 \quad (10)$$

Ferrite with aligned second phase (FAS%)

$$= -0.3141\ CaO + 0.5034\ MgO + 0.0727\ CaF_2 - 0.0957\ Al_2O_3 - 0.0021\ CaO \cdot MgO + 0.0126\ CaO \cdot CaF_2 + 0.0192\ CaO \cdot Al_2O_3 - 0.0123\ MgO \cdot CaF_2 - 0.0095\ MgO \cdot Al_2O_3 - 0.0030\ CaF_2 \cdot Al_2O_3 \quad (11)$$

References

1. "Submerged Arc Welding." Chap. 6 In *Welding Process*. AWS welding handbook, Vol. 2. 8th Ed. American Welding Society: USA, 1992; 182–232.
2. Davis, M.L.E.; Coe, F.R. *The Welding Institute Research Report 39/1977/M*. The Welding Institute: Cambridge, England, May 1977; 1–61.
3. Glover, A.G.; McGrath, J.T.; Trukler, M.J.; Weatherly, G.C. The influence of cooling rate and composition on weld metal microstructure in C–Mn and HSLA steel. Welding Journal **1977**, *56*, 267–273.
4. Davis, M.L.E.; Bailey, N. "Have We the Right Ideas About Fluxes?" Paper 19 In *Proceedings of the International Conferences on Trends in Steels and Consumables for Welding*; The Welding Institute: London, November, 1978; 231–247.
5. North, T.H.; Bell, H.B.; Nowicki, A.; Cray, I. Slag/metal interaction, oxygen and toughness in submerged arc welding. Welding Journal **1978**, *57*, 63–75.
6. Chai, C.S.; Eagar, T.W. Slag/metal reactions in binary CaF_2-metal oxide welding fluxes. Welding Journal **1982**, *61*, 229–232.
7. Indacochea, J.E.; Blander, M.; Christensen, N.; Olson, D.L. Chemical reactions during submerged arc welding with FeO–MnO–SiO_2 fluxes. Metallurgical Transactions **1985**, *16B*, 237–245.
8. Natalie, C.A.; Olson, D. L.; Blander, M. "Weld-pool pyrometallurgy." Chap. 5. In *Welding: Theory and Practice*; Elsevier Science Publishers: Amsterdam, 1990; 151–173.
9. Moor, M.A.B.; North, T.H.; Bell, H.B. Characteristic properties of flux formulation used in submerged arc welding. Welding and Metal Fabrication **1978** (April), 193–199.
10. Lau, T.; Weatherly, G.C.; Molern, A. The source of oxygen and nitrogen contamination in submerged arc welding using CaO-Al_2O_3 based fluxes. Welding Journal **1985**, *64*, 343–347.
11. Kanjilal, P.; Majumdar, S.K.; Pal, T.K. Prediction of submerged arc weld-metal composition from flux ingredients with the help of statistical design of mixture experiment. Scandinavian Journal of Metallurgy **2004**, *33*, 146–159.
12. Grong, O.; Matlock, D.K. Microstructural development in mild and low alloy steel weld metal. International Metals Review **1986**, *31* (1), 27–48.
13. Jang, J.; Indacochea, J.E. Inclusion effects on submerged arc weldmetal microstructures. Journal of Material Science **1987**, *22*, 689–700.
14. Dallam, C.B.; Liu, S.; Olson, D.L. Flux composition dependence of microstructure and toughness of submerged arc HSLA weldments. Welding Journal **1985**, *64*, 140–150.
15. Yun, P.; Wuzhu, C.; Zuze, X. Study of high toughness ferrite wire for submerged arc welding of pipeline steel. Material Characterization **2001**, *47*, 67–73.
16. Liu, S.; Olson, D.L. The role of inclusions in controlling HSLA steel weld microstructures. Welding Journal **1986**, *65*, 139–149.
17. Basu, B.; Raman, R. Microstructural variations in a high strength structural steel weld under iso-heat input conditions. Welding Journal **2002**, *81*, 239–248.
18. Kiruma, T.; Hisada, M.; Fuzisawa, S.; Yokoyama, Y.; Katori, S. Steel plates for architectural construction with excellent toughness in large heat input welded joints. Kawasaki Steel Giho **2002**, *34* (4), 153–158.
19. Oldland, P.T.; Ramsay, C.W.; Mattock, D.K.; Olson, D.L. Significant features of high-strength steel weld metal microstructures. Welding Journal **1989**, *68*, 158–168.
20. North, T.H.; Bell, H.B.; Nowicki, A.; Cray, I. Slag/metal interaction, oxygen and toughness in submerged arc welding. Welding Journal **1978**, *57*, 65–75.
21. Kanjilal, P.; Majumdar, S.K.; Pal, T.K. Weld metal microstructure prediction in submerged arc weld metal of C–Mn steel. Accepted for publication in the Journal "Steel research International" in April or May 2006.
22. McLean, R.A.; Anderson, V.L. Extreme vertices design of mixture experiments with mixture. Technometrics **1966**, *8*, 447–454.
23. Snee, R.D.; Marquardt, D.W. Screening concepts and designs for experiments with mixture. Technometrics **1976**, *18*, 19–29.
24. Snee, R.D.; Marquardt, D.W. Extreme vertices designs for linear mixture models. Technometrics **1974**, *16*, 399–408.
25. Snee, R.D. Experimental design of mixture systems with multicomponent constraints. Communications in Statistics: Theory and Methods **1979**, *48* (4), 303–326.
26. "Standard methods for tension testing of metallic materials (metric)." Section 3, In *Annual Book of ASTM Standards*; ASTM Designation: E8M-1985, 152–175.

27. "Standard methods for notched for impact testing of metallic materials." Section 3, In *Annual Book of ASTM standards*; Vol. 03.01, ASTM Designation: E 23-1985, 235–258.
28. Tuliani, S.S.; Boniszewski, T.; Eaton, N.F. Notch toughness of commercial submerged arc weld metal. Welding and Metal Fabrication **1967**, *37*, 327–339.
29. Abson, D.J. The role of inclusions in controlling weld metal microstructures in C–Mn steels. *The Welding Institute Research Report 69/1978/M*. The Welding Institute: Cambridge, UK, July, 1978.
30. Barritte, G.S.; Edmonds, D.V. Proceedings of *Advances in the Physical Metallurgy of Steel*; The Metals Society: Liverpool. London, 1981; 126–135.
31. Evans, G.M.: The effect of manganese on the microstructure and properties of all-weld metal deposits, (IIW Document No. IIW/IIS 11-A-432-77) Welding Journal **1981**, *60*, 67–75.
32. Garland, J.G.; Kirkwood, P.R. Towards improved submerged arc weld metal, Part 1 in Metal Construction 1975, May, 275–281 and Part 2 in Metal Construction 1975, June, 320–330.
33. Dolby, R.E. Factors controlling weld toughness. The present position, Part 2. Weld metals. In *The Welding Institute Research Report: 14/1976/M*. The Welding Institute, May 1976; 1–17.
34. Kanjilal, P., Pal, T.K., Majumdar, S.K. Prediction of Acicular ferrite from flux ingredients in submerged arc weld metal of C–Mn steel. ISIJ International **2005**, June, 876–884.